Conductivity of disordered 2d binodal Dirac electron gas: effect of internode scattering

Andreas Sinner and Klaus Ziegler

Institut für Physik, Universität Augsburg, Augsburg, Germany

ABSTRACT

We study the dc conductivity of a weakly disordered 2d Dirac electron gas with two bands and two spectral nodes, employing a field theoretical version of the Kubo–Greenwood conductivity formula. In this paper, we are concerned with the question how the internode scattering affects the conductivity. We use and compare two established techniques for treating the disorder scattering: The perturbation theory, there ladder and maximally crossed diagrams are summed up, and the functional integral approach. Both turn out to be entirely equivalent. For a large number of random potential configurations we have found only two different conductivity scenarios. Both scenarios appear independently of whether the disorder does or does not create the internode scattering. In particular, we do not confirm the conjecture that the internode scattering tends to Anderson localisation.

1. Introduction

Transport in two-dimensional (2d) electronic systems has been a subject of intense research for several decades. One of the reasons for the attractiveness of this field is that quantum interference is strong in 2d and interesting phenomena emerge, such as the quantum Hall effect. Despite of its long history, some aspects of electronic transport are still puzzling. For some time there was a consensus about the role disorder plays in transport processes, dominated by Anderson localisation of electronic wave functions for conventional 2d systems [1–4]. A first hint, though, for an unconventional behaviour was the transition between Hall plateaux in quantum Hall systems, which indicated the existence of a metallic state in a 2d electronic system under special conditions [5]. Even more important was the discovery of metallic states in graphene [6–8] and in a number of chemical compounds, which are commonly referred to as topological insulators [9–12], where the band structure has nodes and the electronic dispersion is linear in the vicinity of these nodes. Although these compounds represent pristine 2d systems, they reveal a finite dc conductivity which is very robust against thermal

fluctuations and disorder. In the course of subsequent years, these systems underwent careful studies from both the experimental and the theoretical point of view which clearly indicate that the finite dc value is a robust property.

The theoretical approach to the dc conductivity of disordered electron gases represents a notoriously difficult problem. The presence of disorder breaks explicitly the translational invariance, which obscures most of the tools of pristine microscopic analysis. An alternative way follows via the restoration of the translational invariance by averaging the observable quantity of interest over all disorder configuration. In practice though, the averaging of that sort can only be performed under assumption of a weak disorder, which guarantees for a well formed saddle-like shape of the free energy functional. Consequently, the calculations can be performed either in the Hamiltonian framework, which implies a partial summation of perturbative series in powers of random potential [2–4,13–23], or in Lagrangian framework, where the structure of elementary excitations around the saddle point in a functional integral and the related field theoretical non–linear sigma models become the main object of studies [24–37]. In the course of several years both approaches developed themselves into independent branches of physics and are seldom compared directly with each other. Besides a detailed analysis of the transport properties of systems with a nodal spectrum, the comparison of different approximative approaches is a central goal in this paper.

This paper aims at the understanding of the effects of different scattering types in systems with a nodal electronic spectrum at chemical neutrality. Previous studies are inconclusive on the role intra- and internode scattering processes may play in electronic transport, ranging from essentially no difference [13] to strong statements about a localisation–antilocalisation transition [14–17], while general symmetry arguments indicate that massless modes should survive in the presence of random internode scattering [38,39].

We pursue a two–stage program, starting with the discussion of the averaging procedure based on the combination of functional integrals for quasiparticles with different statistics. This leads us to an effective field theory in terms of graded matrix fields. The nontrivial vacuum of this theory turns out to be identical with the self-consistent Born approximation which is employed in the later parts of the paper. The inverse propagator of the effective action, obtained as Gaussian fluctuations around this vacuum, turns out to be identical, up to a unitary transformation, with the solutions of the Bethe–Salpeter equation. In the second part of the program, we develop further the weak scattering formalism, formulated in our recent papers [38–44]. Besides the already mentioned comparison of two approaches, we calculate the conductivity for 16 different disorder types. We detect two apparently different conductivity scenarios, which we call Type I and II scenario. The conductivity in first scenario arises solely from the channel of ladder diagrams (LC–channel), which includes all diagrams without intersecting impurity lines, while the contribution from the channel of maximally

crossed diagrams (MC–channel) is zero. In the second case, the MC-channel gives rise to the conductivity, while the contribution from the LC-channel is zero. Nonetheless, the evaluation of the Bethe–Salpeter equation with the self–consistent evaluation of the scattering rate reveals the presence of massless modes in both channels for nearly all disorder types but with different degeneracy. This indicates that not all massless modes contribute to the Kubo–Greenwood formula. Our analysis does not confirm the widespread perception that the discrete symmetries of the Hamiltonian determines uniquely the transport properties. In particular, we do not observe any unique correlations between the Cartan class of a particular random Hamiltonian with its dc conductivity calculated from the Kubo–Greenwood formula. This is in line with previous observations [53,54].

The scope of this paper is as follows: In Section 2 we introduce the effective model which is studied subsequently. Apart from the tight–binding approximation for non–interacting electrons on a 2d bipartite lattice, which yields a degenerated linear Dirac spectrum in the low–energy domain, we discuss the phenomenology of different types of scattering in a random potential landscape. Furthermore we introduce and explain the conductivity Kubo–Greenwood formula based on the density–density correlation function [32,40–46], which is evaluated in the course of this work. The link between this version of the Kubo–Greenwood formula and diffusion is briefly discussed in Appendix 1. In Section 3 we study the Gaussian fluctuations of the model within a functional integral approach, based on the notion of an intrinsic graded symmetry of the two–particle Green's function. Some technical details are moved into Appendices 2 and 3. We continue in Section 4 and in Appendix 4, where we approach the conductivity of the model by employing the perturbative averaging technique. We obtain generic expressions for the conductivity regardless of the disorder type and evaluate it for 16 different types in Section 5. In Section 6 we discuss the obtained results in comparison to some alternative approaches.

2. Model

The dynamics of free electrons on bipartite lattices is governed by the family of tight–binding Hamiltonians

$$H_0 = -t \sum_{\langle rr' \rangle} \left(c_r^\dagger d_{r'} + d_{r'}^\dagger c_r \right) , \tag{1}$$

where c and d ($c^\dagger$ and $d^\dagger$) are the fermionic annihilation (creation) operators with respect to each sublattice of a bipartite lattice, respectively. The neighbouring lattice sites r and r' are connected with the hopping amplitude t, and the summation is performed over nearest neighbour pairs only. Although we ultimately consider the case of the honeycomb lattice with the Fermi energy laying at the nodal points, the analysis is valid for other types of bipartite lattices as well. The Hamiltonian is readily diagonalised by Fourier transformation and yields on a honeycomb

lattice a well–known spectrum with two nodes. As a striking feature, close to these nodes the fermion dispersion is linear and therefore describes massless Dirac particles [47,48]. In order for the Hamiltonian to remain invariant under the time–reversal transformation both Dirac cones must be linked to each other by a parity transformation, i.e. they have different chiralities. Sometimes, the gas of such electrons at chemical neutrality is called the Weyl semimetal [49]. The effective low–energy Hamiltonian accounts for both Dirac species and reads [47,48]

$$H_0 \simeq v_F \begin{pmatrix} p_1\sigma_1 + p_2\sigma_2 & 0 \\ 0 & p_1\sigma_1 - p_2\sigma_2 \end{pmatrix} \equiv v_F \begin{pmatrix} h & 0 \\ 0 & \sigma_3 h^T \sigma_3 \end{pmatrix} = v_F(p_1\Sigma_{01} + p_2\Sigma_{32}) \,, \tag{2}$$

where matrices $\Sigma_{ij} = \sigma_i \otimes \sigma_j, \sigma_{i,j}$ are the unity ($i,j = 0$) and 3 Pauli ($i,j = 1,2,3$) matrices in the usual representation, the momentum operators are $p_i = -i\hbar\nabla_i$, v_F denoting the Fermi velocity. Below we use dimensionless energy units, i.e. $\hbar v_F = 1$ in units of inverse length.

Disorder appears in the model in form of one–particle random potentials V which are matrices in the Dirac space. Due to the mentioned nodal degeneracy in the electronic spectrum, all possible disorder scattering processes can be roughly subdivided into those with and without mixing of electrons with different chiralities. The former processes are referred to as the intranode scattering. Corresponding random low–energy Hamiltonians have the diagonal block structure

$$H = \begin{pmatrix} h + V_+ & 0 \\ 0 & \sigma_3 h^T \sigma_3 + V_- \end{pmatrix} , \tag{3}$$

where $V_\pm$ denotes the random part, i.e. each block can be diagonalised independently. On the other hand, electrons whose scattering involves a change of the chirality are referred to as internode scattering processes. Corresponding Hamiltonians have the following generic form

$$H = \begin{pmatrix} h_+ & V \\ V^* & \sigma_3 h_+^T \sigma_3 \end{pmatrix} . \tag{4}$$

The Hamiltonian can also be written as $H = H_0 + V$ with the 4×4 random matrix

$$V = v_{ij}\Sigma_{ij}, \tag{5}$$

where v_{ij} is the random coordinate-dependent part and the summation convention is used. Then, the decomposition coefficients with $i = 0,3$ are those responsible for the intra-node scattering, while $i = 1,2$ is for inter-node scattering. In this paper we concentrate on a somewhat simpler model, where each disorder type has a decomposition with one term only; i.e.

$$V = v\Sigma_{ij}, \quad i,j \text{ fixed.} \tag{6}$$

In a usual fashion, we assume for the random part of the disorder potential a Gaussian distribution independently for each site with

$$\langle v(r)\rangle_g = 0, \qquad \langle v(r)v(r')\rangle_g = g\delta(r-r'), \tag{7}$$

where g is referred to as the disorder strength and $\langle\cdots\rangle_g$ denotes the ensemble averaging. Then the disorder strength is measured in units of $(\hbar v_F)^2$ and the quantity $s = (\hbar v_F)^2$ represents an appropriate reference scale.
Special cases: The case $V_+ = -V_- = \mu\sigma_0$ (i.e. for Σ_{30} disorder) is equivalent (up to an orthogonal transformation) to a single Dirac with random scalar potential [45]. Moreover, the case of Σ_{03} is related to the random gap model [35,36]. The latter has only one massless mode, corresponding to a massless fermion mode in the functional integral [29–31] or to a maximally crossed diagram in the weak perturbation series [38].

2.1. The Kubo–Greenwood conductivity formula

Motivated by the phenomenon of diffusion at large times [26,37,50] (cf. Appendix 1), we consider the field theoretical version of the Kubo–Greenwood conductivity formula

$$\bar{\sigma}_{\mu\mu} = \frac{e^2}{h}\lim_{\epsilon\to 0}\int \mathrm{d}E\,\Gamma_\mu(E,\epsilon)\,\frac{f(E)-f(E+i\epsilon)}{i\epsilon}, \tag{8}$$

where $f(E)$ is the Fermi function, ϵ is the zero–temperature Matsubara frequency, and the disorder averaged core function reads

$$\Gamma_\mu(E,\epsilon) = \epsilon^2 \mathrm{Tr}_d \sum_r r_\mu^2\,\langle G^+(r,0)G^-(0,r)\rangle_g, \tag{9}$$

where $G^+(r,r')$ ($G^-(r,r')$) denotes the microscopic advanced (retarded) single–particle Green's function at energy E analytically continued into the upper (lower) halfplane

$$G^\pm(r,r') = \langle r|[E\pm i\epsilon + H_0 + V]^{-1}|r'\rangle. \tag{10}$$

The operator Tr_d denotes the trace operator on the space of d–dimensional Green's functions. At frequencies small as compared to the typical band width of the clean system and well below room temperature we can employ the usual approximation $f(E+i\epsilon) \sim f(E) + i\epsilon\delta(E)$, which trivialises the energy integral in Equation (8). Then the conductivity formula becomes

$$\bar{\sigma}_{\mu\mu} = \lim_{\epsilon\to 0}\epsilon^2\left(-\frac{\partial^2}{\partial q_\mu^2}\right)\Bigg|_{q=0}\sum_r e^{iq\cdot r}\langle G^+_{ij}(r,0)G^-_{ji}(0,r)\rangle_g, \tag{11}$$

where we have used the Fourier representation of the position operator and the summation convention for matrix elements with respect to the spinor index. Due to the randomness each realisation of the system lacks translational invariance and the Green's function depends on both sites r and r'. The establishing of the translational invariance is achieved by the averaging procedure. In Sections 3 and 4, we demonstrate how the averaging is performed within a functional–integral formalism and a diagrammatic weak–scattering formalism, respectively.

3. Functional integral approach

The functional integral approach to disorder averaged quantities and eventually to the conductivity can be based on a functional integral with a fermionic and a bosonic field. Usually, the propagators for both fields are identical, and the functional integral is called supersymmetric [22]. An alternative to this supersymmetric functional integral is based on the identity between the determinants of two different Green's functions [29–31,35–37]

$$\det G = \det G' \,. \tag{12}$$

Then we can use the Green's function G for the fermionic field and G' for the bosonic field (or vice versa) and calculate the average product $\langle GG' \rangle$ within this functional-integral representation. In our specific case, we have the determinant identity (cf. Appendix 2)

$$\det[i\epsilon + H_0 + V] = \det[i\epsilon + H_0^T - \mathcal{O}V\mathcal{O}] \,, \tag{13}$$

where H_0^T describes the Hamiltonian transposed on all spaces and the operator $\mathcal{O}$ satisfies the condition

$$H_0 = -\mathcal{O}H_0^T\mathcal{O}. \tag{14}$$

For the Dirac Hamiltonian it is important to notice the transposition rule of the momentum operator: $p_i^T = -p_i$, due to the property of the differential operator $\partial_{x_i}^T = \partial_{-x_i} = -\partial_{x_i}$. Therefore with $H_0 = p_1\Sigma_{01} + p_2\Sigma_{32}$ follows $H_0^T = -p_1\Sigma_{01} + p_2\Sigma_{32}$ and either $\mathcal{O} = \Sigma_{01}$ or $\mathcal{O} = \Sigma_{31}$. The identity (13) is valid for the Dirac Hamiltonian in Equation (2) and for any random potential $V = v\Sigma_{ij}$ obeying $\mathrm{Tr}_d V = 0$. The latter condition rules out the totally degenerated random potential $V = v\Sigma_{00}$, which is discussed separately in Appendix 3.

The identity (13) allows us to write the disorder averaged of two-particle Green's function in Equation (27)

$$\begin{aligned} K_{rr'} &= \mathrm{Tr}_d \left\langle [i\epsilon + H_0 + V]^{-1}_{rr'} [-i\epsilon + H_0 + V]^{-1}_{r'r} \right\rangle_g \\ &= -\mathrm{Tr}_d \left\langle [i\epsilon + H_0 + V]^{-1}_{rr'} \mathcal{O} [i\epsilon + H_0^T - \mathcal{O}V\mathcal{O}]^{-1}_{r'r} \mathcal{O} \right\rangle_g \\ &= \mathcal{O}_{jk}\mathcal{O}_{li} \left\langle \chi_{r,kj} \bar{\chi}_{r',il} \right\rangle_{\hat{Q}} \,. \end{aligned} \tag{15}$$

For the last equation we have used a functional integral with respect to the matrix field

$$\hat{Q} = \begin{pmatrix} Q & \chi \\ \bar{\chi} & iP \end{pmatrix} . \tag{16}$$

The 4×4 matrices Q, P with commuting elements, and $\bar{\chi}, \chi$ with anticommuting elements are hermitian, and thus can be expanded in a basis which includes a four–dimensional unity matrix and 15 traceless matrices, which are fifteen Γ–matrices. The functional integral is defined as

$$\langle \cdots \rangle_{\hat{Q}} = \int \cdots e^{-\mathcal{S}_G} \prod_r d\bar{\chi}_r d\chi_r dQ_r dP_r \tag{17}$$

with the action $\mathcal{S}_G$

$$\mathcal{S}_G[\hat{Q}] = \frac{1}{2} \mathrm{Trg} \int d^2r d^2r' \left\{ \frac{1}{g} \delta_{rr'} \hat{Q}_r \hat{Q}_{r'} - \hat{G}(r, r') \hat{Q}_{r'} \hat{\Sigma} \hat{G}(r', r) \hat{Q}_r \hat{\Sigma} \right\} \tag{18}$$

and with frequency- and position-dependent Green's functions

$$\hat{G}(r, r') = \left\langle r | [iz + \hat{H}_0]^{-1} | r' \right\rangle, \tag{19}$$

where $\hat{H}_0 = \mathrm{diag}[H_0, H_0^T]$, $H_0 = p_1 \Sigma_{01} + p_2 \Sigma_{32}$, and $z = \epsilon + \eta$. The operator Trg denotes the graded trace with $\mathrm{Trg}\hat{Q} = \mathrm{Tr}Q - i\mathrm{Tr}P$. Equation (18) is the result of the saddle-point approximation of a more complex functional integral, taking only fluctuations up to quadratic (Gaussian) order into account. The saddle point equation reads

$$\frac{i\eta}{g} = -\int \frac{d^2q}{(2\pi)^2} \left[iz + \hat{H}_0 \right]^{-1} = \int \frac{d^2q}{(2\pi)^2} \frac{iz}{z^2 + q^2}. \tag{20}$$

The action in Equation (18) can be decomposed into bosonic and fermionic sectors: $\mathcal{S}_G = \mathcal{S}[Q] + \mathcal{S}[P] + \mathcal{S}[\bar{\chi}, \chi]$. Expanding the kernel of the bilinear expression in powers of the momentum of the field (equivalent to a gradient expansion in real space), we obtain at zeroth order

$$\mathcal{S}[Q] = \frac{1}{2g} \int \frac{d^2q}{(2\pi)^2} \, Q_{ab}(q) M^{Q}_{a\alpha,b\beta} Q_{\alpha\beta}(-q), \tag{21}$$

$$\mathcal{S}[P] = \frac{1}{2g} \int \frac{d^2q}{(2\pi)^2} \, P_{ab}(q) M^{P}_{a\alpha,b\beta} P_{\alpha\beta}(-q), \tag{22}$$

$$\mathcal{S}[\bar{\chi}, \chi] = \frac{1}{g} \int \frac{d^2q}{(2\pi)^2} \, \bar{\chi}_{ab}(q) M^{\chi}_{a\alpha,b\beta} \chi_{\alpha\beta}(-q) \tag{23}$$

with

$$M^{Q}_{a\alpha,b\beta} = \delta_{\alpha b}\delta_{a\beta} - g\int \frac{d^2p}{(2\pi)^2}\left[\Sigma_B G^{-}(p)\right]_{\beta a}\left[\Sigma_B G^{-}(p)\right]_{b\alpha}, \tag{24}$$

$$M^{P}_{a\alpha,b\beta} = \delta_{\alpha b}\delta_{a\beta} - g\int \frac{d^2p}{(2\pi)^2}\left[\mathcal{O}\Sigma_B G^{+}(p)\mathcal{O}\right]_{\beta a}\left[\mathcal{O}\Sigma_B G^{+}(p)\mathcal{O}\right]_{b\alpha}, \tag{25}$$

$$M^{\chi}_{a\alpha,b\beta} = \delta_{\alpha b}\delta_{a\beta} - g\int \frac{d^2p}{(2\pi)^2}\left[\Sigma_B G^{-}(p)\right]_{\beta a}\left[\mathcal{O}\Sigma_B G^{+}(p)\mathcal{O}\right]_{b\alpha} \tag{26}$$

with $G^{\pm}(p) = [\pm i\eta + H_0]^{-1}$. Note the missing combinatorial factor 1/2 in $\mathcal{S}[\bar{\chi}, \chi]$, since it counts both permutations $\bar{\chi}\chi$ and $\chi\bar{\chi}$. Once the fluctuations in Equation (21)–(23) are expressed as quadratic forms in terms of real valued expansion coefficients of fields $Q, P, \bar{\chi}$,and χ,the eigenvalues of the corresponding inverse propagator matrices become nonnegative.

The expansion of Equation (18) to second order in the momenta yields the inverse (diffusion) propagators. This enables us to compare the functional-integral approach with a weak-scattering expansion of Section 4. In particular, the expression for zero momentum, which represents the mass matrices, has non-zero eigenvalues. Zero eigenvalues are most important, since they correspond to diffusion modes.

4. Perturbative averaging approach to the conductivity

In the second part of our program, we approach the dc conductivity within a weak scattering approach, in which the disorder average is performed perturbatively. This is the standard method in the weak–localisation approach, in which the Green's functions are expanded in terms of the random scattering elements and averaged afterwards [2–4,13–23]. As an extension of the analysis in our recent papers [38,39], where we were concerned with the conductivity behaviour in the single-cone approximation, here we take both cones into account. The averaged two-particle Green's function

$$K_{rr'} = \left\langle G^{+}_{nj}(r,0)G^{-}_{jn}(0,r)\right\rangle_g \tag{27}$$

is treated within a perturbative expansion in powers of weak scattering rate η, which plays the role of the order parameter in diffusive regime. It is determined self-consistently from

$$\pm i\eta = -\frac{1}{d}\sum_{r'}\mathrm{Tr}_d\left\langle V(r)G^{\pm}(r,r')V(r')\right\rangle_g = -\frac{g}{d}\mathrm{Tr}_d\left[\Sigma\bar{G}^{\pm}(r,r)\Sigma\right], \tag{28}$$

where Σ are disorder matrices in Dirac space. The averaged one-particle Green's functions become translationally invariant and read

$$\bar{G}^{\pm}(r,r') = \langle r|[\pm iz + H_0]^{-1}|r'\rangle = \int \frac{d^2p}{(2\pi)^2}\, e^{ip(r-r')} \frac{\tilde{H}_0 \mp iz}{p^2+z^2}, \tag{29}$$

with $z = \epsilon + \eta$ and $\tilde{H}_0$ denoting the Fourier-transformed Hamiltonian. $\tilde{H}_0$ is not rotational invariant and does not contribute to the integral. We recognise then in Equation (28) the saddle point of the functional integral defined in Equation (20). For $\epsilon \sim 0$ we get

$$1 - \int \frac{d^2p}{(2\pi)^2} \frac{g}{p^2+z^2} \sim \frac{\epsilon}{\eta}. \tag{30}$$

Partial summations of all ladder (LC) and maximally crossed (MC) diagrams (see Appendix 4) lead to

$$\begin{aligned}\bar{\sigma}_{\mu\mu} = \lim_{\epsilon\to 0}\, \epsilon^2 \left(-\frac{\partial^2}{\partial q_\mu^2}\right)\Bigg|_{q=0} \sum_{rr'} e^{iq\cdot r}\, \bar{G}^{+}_{ij}(r',0)\bar{G}^{-}_{kn}(0,r') \\ \times \Big[\left(1 - g[\bar{G}^{+}\Sigma][\bar{G}^{-}\Sigma]\right)^{-1}_{rr'|nj;ik} \\ + \left(1 - g[\bar{G}^{+}\Sigma][\bar{G}^{-}\Sigma]^T\right)^{-1}_{rr'|nk;ij}\Big],\end{aligned} \tag{31}$$

where the full transposition operator T applies to all degrees of freedom. We shall call the terms in the second line of Equation (31)

$$\text{(a) } t = g\left[\bar{G}^{+}\Sigma\right]\left[\bar{G}^{-}\Sigma\right], \quad \text{(b) } \tau = g\left[\bar{G}^{+}\Sigma\right]\left[\bar{G}^{-}\Sigma\right]^T \tag{32}$$

the LC (Equation (32a)) and the MC (Equation (32b)) channel matrices, respectively [38]. These matrices read in Fourier representation

$$\begin{aligned} t_{r'r|ab;cd} &= g\int \frac{d^2q}{(2\pi)^2}\, e^{-iq\cdot(r-r')} \\ &\quad\times \int \frac{d^2p}{(2\pi)^2}\, [\bar{G}^{+}(p)\Sigma]_{ac}\left[\bar{G}^{-}(q+p)\Sigma\right]_{bd}, \end{aligned} \tag{33}$$

$$\begin{aligned} \tau_{r'r|ab;cd} &= g\int \frac{d^2q}{(2\pi)^2}\, e^{-iq\cdot(r'-r)} \\ &\quad\times \int \frac{d^2p}{(2\pi)^2}\, [\bar{G}^{+}(p)\Sigma]_{ac}[\bar{G}^{-}(q-p)\Sigma]_{db}. \end{aligned} \tag{34}$$

The different signs in the argument of t and τ are a consequence of the transposition on the position space in the MC–channel. Fourier transformed matrices $1 - \tilde{t}_q$ and $1 - \tilde{\tau}_q$ for $\epsilon = 0$ and $q = 0$ read

$$M^{LC}_{ab;cd} = \delta_{ac}\delta_{bd} - g\int \frac{d^2p}{(2\pi)^2}\,[\bar{G}^+(p)\Sigma]_{ac}[\bar{G}^-(p)\Sigma]_{bd}\Big|_{\epsilon=0}, \tag{35}$$

$$M^{MC}_{ab;cd} = \delta_{ac}\delta_{bd} - g\int \frac{d^2p}{(2\pi)^2}\,[\bar{G}^+(p)\Sigma]_{ac}[\bar{G}^-(-p)\Sigma]_{db}\Big|_{\epsilon=0}. \tag{36}$$

Matrices M in Equations (35) and (36) are diagonalised by the momentum independent orthogonal transformations O. The eigenvalues of the matrices M provide a decay length for the matrices in Equation (32). In particular, a vanishing (e.g. gapless) eigenvalue gives a long-range diffusion-like behavior. Depending on the type of disorder there may or may not be gapless modes. If gapless modes exist, then for small momenta and frequencies we get in the LC channel (in the channel of MC diagrams analogously)

$$\begin{aligned} t_{r'r} &\sim O_{LC}\,\mathrm{diag}[t]_{r'r}\,O^T_{LC} \\ &\sim \int \frac{d^2q}{(2\pi)^2}\,e^{iq\cdot(r-r')}\,O_{LC}\begin{bmatrix}\left(\dfrac{\epsilon}{\eta}+gD_0q^2\right)1_N & \mathbf{0}^T \\ \mathbf{0} & \hat{\Lambda}_{D-N}\end{bmatrix}O^T_{LC}, \end{aligned} \tag{37}$$

where N is the dimension of the subspace populated by gapless modes. $\hat{\Lambda}_{D-N}$ represents the diagonal matrix with non–zero eigenvalues of M^{LC} as matrix elements. D is the dimension of the full space on which the product $G^+ \otimes G^-$ dwells, and D_0 is the expansion coefficient, which fortunately turns out to be the same for all studied cases:

$$D_0 = \frac{1}{2}\int \frac{d^2p}{(2\pi)^2}\,\frac{1}{[p^2+\eta^2]^2} \sim \frac{1}{8\pi\eta^2}. \tag{38}$$

Finally, $\mathbf{0}$ is an $(D-N)\times N$ matrix whose elements are zero. Using the convolution formula for the tensor product of two Green's functions

$$\bar{G}^+_{ij}(r,0)\bar{G}^-_{kn}(0,r) = \int \frac{d^2p}{(2\pi)^2}\,e^{-ip\cdot r}\int \frac{d^2k}{(2\pi)^2}\,\bar{G}^+_{ij}(k)\bar{G}^-_{kn}(k+p), \tag{39}$$

we can bring Equation (31) to the form where the derivatives with respect to the external momentum q can be easily evaluated. After performing the dc limit we arrive at

$$\begin{aligned} \bar{\sigma}_{\mu\mu} = 2g\eta^2 D_0 \int \frac{d^2p}{(2\pi)^2}\,\bar{G}^+_{ij}(p)\bar{G}^-_{kn}(p) \\ \times\left\{\left[O_{LC}\begin{pmatrix}1_{N_{LC}} & \mathbf{0}^T \\ \mathbf{0} & \hat{\mathbf{0}}_{D-N_{LC}}\end{pmatrix}O^T_{LC}\right]_{nj;ik}\right. \\ \left.+\left[O_{MC}\begin{pmatrix}1_{N_{MC}} & \mathbf{0}^T \\ \mathbf{0} & \hat{\mathbf{0}}_{D-N_{MC}}\end{pmatrix}O^T_{MC}\right]_{nk;ij}\right\}, \end{aligned} \tag{40}$$

Table 1. Eigenvalues and their number of the mass matrices in LC channel for the random potentials $v\,\Sigma_{ij}$ giving Type I conductivity.

Matrix Σ_{ij}	0	a	2a	2b	2(a + b)	a + 2b
Σ_{00}	4	8	4	0	0	0
Σ_{01}	4	4	0	4	0	4
Σ_{02}	2	4	2	2	2	4
Σ_{30}	2	4	2	2	2	4
Σ_{31}	2	4	2	2	2	4
Σ_{32}	4	4	0	4	0	4
Σ_{10}	2	4	2	2	2	4
Σ_{11}	2	4	2	2	2	4
Σ_{13}	2	4	2	2	2	4
Σ_{20}	2	4	2	2	2	4
Σ_{21}	2	4	2	2	2	4
Σ_{23}	2	4	2	2	2	4

Note: a and b are defined in Equation (50)

Table 2. Eigenvalues and their number of the mass matrices in LC channel for the random potentials $v\,\Sigma_{ij}$ giving Type II conductivity.

Matrix Σ_{ij}	0	a	2a	2b	2(a + b)	a + 2b
Σ_{03}	2	4	2	2	2	4
Σ_{33}	0	8	0	4	4	0
Σ_{12}	2	4	2	2	2	4
Σ_{22}	2	4	2	2	2	4

Note: a and b are defined in Equation (50)

where $\hat{\mathbf{0}}_{D-N}$ denotes a $(D-N)\times(D-N)$ zero matrix. This result indicates that the conductivity $\bar{\sigma}_{\mu\mu}$ is finite for a positive scattering rate η. In particular, it does not have a logarithmic divergence in the limit of zero temperature, as predicted in some weak localisation calculations. For correct evaluation of the conductivity, the disorder strength parameter g in front of the integral must be compensated with the help of the saddle point condition (30):

$$\int \frac{d^2p}{(2\pi)^2}\,\bar{G}^{+}_{ij}(p)\bar{G}^{-}_{kn}(p)\Gamma_{ikjn} = \frac{1}{g} + \text{remaining terms}, \tag{41}$$

where the quantity Γ denotes the full tensor in the curly brakets. For ultimate values of the conductivity we must determine the orthogonal matrices O_{LC} and O_{MC}. This requires the explicit knowledge of the type of disorder, i.e. matrices Σ. In Section 5, we discuss solutions of Equation (40) for a number of disorder types.

5. Conductivity for different random potentials

Now, we can evaluate the conductivity of a binodal Dirac electron gas in a random potential from Equation (31). In order to investigate the role of the disorder mediated intermixing of Dirac electrons with different chiralities we use the full

Table 3. Eigenvalues and their number of the mass matrices in MC channel for the random potentials $v\,\Sigma_{ij}$ giving Type I conductivity.

Matrix Σ_{ij}	0	a	2a	2b	2(a + b)	a + 2b
Σ_{00}	4	8	4	0	0	0
Σ_{01}	0	4	4	0	4	4
Σ_{02}	2	4	2	2	2	4
Σ_{30}	2	4	2	2	2	4
Σ_{31}	2	4	2	2	2	4
Σ_{32}	0	4	4	0	4	4
Σ_{10}	2	4	2	2	2	4
Σ_{11}	2	4	2	2	2	4
Σ_{13}	2	4	2	2	2	4
Σ_{20}	2	4	2	2	2	4
Σ_{21}	2	4	2	2	2	4
Σ_{23}	2	4	2	2	2	4

Note: a and b are defined in Equation (50)

Table 4. Eigenvalues and their number of the mass matrices in MC channel for the random potentials $v\,\Sigma_{ij}$ giving Type II conductivity.

Matrix Σ_{ij}	0	a	2a	2b	2(a + b)	a + 2b
Σ_{03}	2	4	2	2	2	4
Σ_{33}	4	0	4	0	0	8
Σ_{12}	2	4	2	2	2	4
Σ_{22}	2	4	2	2	2	4

Note: a and b are defined in Equation (50)

renormalised Dirac propagators $\bar{G}^{\pm}(p)$ which read in Fourier representation

$$\bar{G}^{\pm}(p) = \frac{1}{p^2+\eta^2}\begin{pmatrix} \mp i\eta & p_1 - ip_2 & 0 & 0 \\ p_1 + ip_2 & \mp i\eta & 0 & 0 \\ 0 & 0 & \mp i\eta & p_1 + ip_2 \\ 0 & 0 & p_1 - ip_2 & \mp i\eta \end{pmatrix}. \tag{42}$$

Different disorder types were studied by inserting respective disorder matrices Σ_{ij} directly into Equations (31) and then unfolding them up to the form of Equation (40). In all we have evaluated the conductivity for 16 different disorder configurations. Technically, the evaluation of the conductivity contributions for each disorder type does not differ much from the single–cone model evaluation presented in our recent papers Refs. [38,39]. The number of massless modes is obtained by counting zero eigenvalues of the corresponding mass matrices given in Equations (35) and (36). Despite high dimensionality of the matrices (16×16 or even 64×64), the order of the characteristic polynomial is small, since the matrices are sparsely occupied. In the case of 16×16–matrices, of 256 matrix elements only 24 to 32, depending on the disorder type, are non–zero. Moreover, the mass matrices are symmetric. Consequently, they can be diago-

nalised analytically using a computer algebra package. Then, the calculation of the conductivity from Equation (40) can be carried out exactly. Surprisingly, for all 16 types of random matrices we have discovered only two distinct conductivity types. Both types occur for disorder potentials with and without chirality mixing and have their own features:

Type 1: Reveals a total suppression of the contribution from the MC–channel:

$$\sigma_{\mu\mu}^{MC} \sim 0. \tag{43}$$

The conductivity is entirely controlled by the LC–channel, which yields

$$\sigma_{\mu\mu}^{LC} \sim 4\eta^2 D_0 \sim \frac{1}{2\pi}\,. \tag{44}$$

This conductivity type was found for Σ_{00}, Σ_{01}, Σ_{02}, Σ_{30}, Σ_{31}, Σ_{32}, Σ_{10}, Σ_{11}, Σ_{13}, Σ_{20}, Σ_{21}, Σ_{23}.

Type 2: Demonstrates a picture somewhat reciprocal to the Type 1: The conductivity contribution from the LC–channel is fully suppressed

$$\sigma_{\mu\mu}^{LC} \sim 0, \tag{45}$$

while the MC–channel gives

$$\sigma_{\mu\mu}^{MC} \sim 8\eta^2 D_0(1-a), \tag{46}$$

where the parameter a is defined below in Equation (50). The Type 2 conductivity exhibits a logarithmically suppressed conductivity and was found for Σ_{03}, Σ_{33}, Σ_{12}, Σ_{22}.

Having found only two conductivity types, it is natural to expect that the corresponding disorder matrices share some common features. We would expect that the microscopic random Hamiltonians, which lead to the same conductivity type, belong to the same Cartan classes. This property of the random Hamiltonians is usually brought into connection with the expected Anderson localisation transition in the system [51–54]. According to the Altland–Zirnbauer classification of $N \times N$ random matrices, the behaviour of a random Hamiltonian under the time–reversal, particle–hole, and chiral symmetry transformations determines to which Cartan class this Hamiltonian belongs:

$$TH^*T^\dagger = H, \ \text{Time} - \text{reversal} \ \ \text{symmetry} \tag{47}$$

$$CH^TC^\dagger = -H, \ \text{Particle} - \text{hole} \ \ \text{symmetry} \tag{48}$$

$$PHP^\dagger = -H, \ \text{Chiral} \ \ \text{symmetry}\,. \tag{49}$$

Here, H^* denotes the complex conjugate of the Hamiltonian H and H^T its transposition on all spaces. If we extend the $N \times N$ random matrix ensembles by including a spatial Dirac operator, the number of classes increases at least to

17 for the single-node Dirac-like Hamiltonians [53,54] and may increase even further when two nodes and inter–node scattering is included. Therefore, the classification of random Hamiltonians given by Equation (3) remains a great challenge. In the present work, we focus only on the characterisation of the transport properties. We notice that the mass matrices in both LC and MC channels are unique to each disorder matrix Σ_{ij}. The composition of the sets of eigenvalues for each disorder matrix Σ_{ij} (in particular the number of zero eigenvalues) may differ from each other, even if the microscopic Hamiltonians formally belong to the same Cartan class. The sets of eigenvalues of the mass matrices are shown in Tables 1–4 for both channels with the notation

$$a = \int \frac{d^2p}{(2\pi)^2} \frac{gp^2}{[p^2+\eta^2]^2}, \quad b = \int \frac{d^2p}{(2\pi)^2} \frac{g\eta^2}{[p^2+\eta^2]^2}. \tag{50}$$

A systematic property of the eigenvalue sets consists in the total number of zero eigenvalues per LC and MC channels together. There are always four with the only important exclusion of the totally degenerated disorder which couples to the unity matrix on the extended space Σ_{00}. In the latter case the number of zero eigenvalues is doubled; i.e. 8 instead of 4. This observation is linked back to the continuous symmetry on the configuration space which spontaneously breaks down in order to give rise to the gapless excitations is the same for all disorder types [37,38,45]. In the case of Σ_{00}–case the symmetry lives in a space which is twice as large, cf. Appendix 3. This explains the higher number of massless modes. The order parameter in all cases is the scattering rate η.

Within the functional–integral approach we obtain the same sets of eigenvalues for the various disorder types, as summarised in Tables 1–4. A direct correspondence between the modes of LC– and MC–channel on the one hand, and the fermionic and the bosonic field on the other can be obtained for the random matrices with Σ_{01} and Σ_{32}. These cases are related to the Type 1 conductivity (cf. Tables 1 and 2). For Σ_{33}, which is Type 2 conductivity (Tables 3 and 4), the full set of eigenvalues in LC–channel (with no zero eigenvalues) is reproduced in both bosonic (Q and P) channels, while the full set of eigenvalues of MC–channel arises from the fermionic channel. Thus, the full equivalency of both averaging procedures is established.

Since both conductivity types occur due to the spontaneous breaking of the same continuous symmetry, the origin of the different transport properties must be in the discrete transformations of the effective Hamiltonian on the configuration space. These symmetries are difficult to realise within the perturbative approach of Section 4 but can be recognised using functional integral representation which we discussed in Section 3. The generator $\mathcal{T}$ with $\mathcal{T}\mathcal{T} = 1$ can be considered as an effective time–reversal transformation, when it distinguishes Hamiltonian H_0 and the random part V through the following properties:

$$\text{(a) } H_0 = \mathcal{T} H_0^T \mathcal{T}, \quad \text{(b) } V = -\mathcal{T}\mathcal{O}V\mathcal{O}\mathcal{T}\,. \tag{51}$$

Equation (51a) is solved either for $\mathcal{T} = \Sigma_{02}$ or $\mathcal{T} = \Sigma_{32}$. Combining this with the chiral symmetry condition of Equation (14) for the full Hamiltonian we make the following general observation: If a matrix Σ_{ij} obeys both equalities

$$\text{(a) } \Sigma_{ij} = \mathcal{T}\mathcal{O}\Sigma_{ij}\mathcal{O}\mathcal{T}, \text{ and (b) } \Sigma_{ij} = -\mathcal{O}\Sigma_{ij}\mathcal{O}, \tag{52}$$

for $\mathcal{O} = \Sigma_{01}, \mathcal{T} = \Sigma_{32}$, we have

$$\mathcal{T}(H_0^T + \mathcal{O}V\mathcal{O})\mathcal{T} = (H_0 + V)\,. \tag{53}$$

This is valid for all matrices in V which lead to the Type 2 conductivity, (i.e. for $\Sigma_{03}, \Sigma_{33}, \Sigma_{12}, \Sigma_{22}$), which therefore all disobey Equation (51b) while satisfying Equation (52b). On the other hand, none of the corresponding matrices in V for the Type 1 scenario (i.e. for $\Sigma_{00}, \Sigma_{01}, \Sigma_{02}, \Sigma_{30}, \Sigma_{31}, \Sigma_{32}, \Sigma_{10}, \Sigma_{11}, \Sigma_{13}, \Sigma_{20}, \Sigma_{21}, \Sigma_{23}$) fulfill Equations (52) simultaneously. Thus, the relations (52) characterise Type 2 conductivity, the absence of them characterises Type 1 conductivity.

6. Discussion

The vast body of literature which exists on the subject of the disordered Dirac electron gas raises a natural question of how results presented in this paper are related to previous theoretical and experimental findings. Particularly, the weak-localisation approach [2,3,13,16,19] deserves special attention. It is commonly believed to represent the fastest and most natural way to describe the transport in conventional disordered metals. In its essence it allows to compute so-called perturbative quantum corrections to the classical Drude-Boltzmann conductivity and appears in the form of infinite series of Feynman diagrams. Clearly, such an expansion is possible only in the parametric region close to the classical regime; i.e. for weak quantum fluctuations. A contribution to the Kubo formula comes from the velocity–velocity correlation function

$$\sigma_{\mu\mu} \sim \text{tr}\, v_\mu G_+ v_\mu G_-, \tag{54}$$

where $G_+(G_-)$ represents the advanced (retarded) Green's function. It is dominant in Kubo formula of a one-band system [23] and accounts for the most important corrections to the conductivity. In particular, the corrections arising by summing up the so–called maximally crossed diagrams, shown schematically in appendix in Figure D1. The absence of an extended Fermi surface in the half-filled nodal systems has led to the incorrect perception that the 'ladder'-approximation would break down for the nodal systems. Consequently, in the overwhelming majority of investigations which employ the weak-localisation approach, the Dirac electron gas is considered to be doped; i.e. a chemical potential is introduced to create a Fermi circle instead of the Fermi node, which makes it similar to conventional metals. Precisely at the node the reduced Kubo formula in Equation (54) has its limitations, cf. Appendix 5.

However, a closer inspection of the Dirac node reveals that in the Dyson-Schwinger (or self-consistent Born) approximation disorder generates an exponentially small momentum scale $\sim a^{-1} \exp(-2\pi/g)$ for the leading term of the perturbation series [24–28]. This solves the problem of the spurious and unphysical logarithmic singularities found in the expansion around the trivial vacuum with a vanishing density of states of Ref. [58], which was also discussed previously for the band edges in a one-band model some time ago [59,60]. In other words, the self-consistent approximation provides a non-trivial vacuum state with non-zero density of states around which a perturbative expansions appears with finite non-singular terms. The onset of that scale in the density of states for weak disorder is clearly seen numerically [55–57] but also, which is even more important, experimentally [7].

In summary, our approach, based on the expansion around a non-trivial vacuum, reproduces correctly the experimental transport results, whereas the expansion around the vacuum with a vanishing density of states [58] clearly contradicts the latter with a divergent conductivity. This divergency needs to be cut off by an additional artificially introduced scattering time. This step is rather confusing, since even in the classical Boltzmann approach the elastic random scattering creates a finite conductivity.

Fortunately, through the discovery of graphene it became possible to test the various theoretical predictions with experimental measurements. In the past our approach [29–31] has been compared with experimental work, including the seminal article on graphene by Novoselov et al. on graphene [6] and showed good agreement. More recently we also compared our theoretical results for finite-size scaling with experimental results [39], and found excellent agreement. Moreover, we have used two different approaches in this article, namely a functional integral approach based on symmetry considerations (Section 3) and a perturbative approach based on the Bethe-Salpeter equation (Section 4), and the results of both approaches agree.

7. Conclusions

Despite decades of intense research several aspects of the disorder physics are still challenging. Novel low–dimensional materials defy traditional views and reveal a new and hitherto unexpected physics. The dc conductivity of 2d disordered nodal electron gases represents a striking example of that kind. Following the traditional theories it must necessarily disappear in infinite systems no matter how weak the disorder is. Yet the experimental evidence clearly speaks against this perception. Numerous attempts to reconcile those facts ultimately made the internode scattering processes responsible for localisation. According to this hypothesis, once such processes are realised in the physical systems, it must inevitably become an insulator.

In this work, we performed an extensive studies of the dc conductivity of chemically neutral disordered 2d binodal Dirac or Weyl electron gas aiming at the question, how the internodal scattering affects the transport in such systems. Using the version of the Kubo–Greenwood formula based on the density–density correlation function, we compared two technically very different approaches to the disorder averaging: the perturbative weak scattering technique and the non–perturbative functional integral approaches. For a large number of disorder potentials we obtained from both approaches the same diffusion propagators, which eventually give rise to the conductivity. Our findings reveal a very simple picture of what happens in those systems. There are only two distinct conductivity types, the one which yields a universal conductivity value in infinite systems and the second which reveals a logarithmically suppressed conductivity. However, in contrast for instance to the weak–localisation theory, even in the latter case Anderson localisation never occurs and the system remains a conductor. The internode scattering can be definitely ruled out as the primary cause of the localisation in nodal systems, since both conductivity types are observed for both inter- and intranode scattering potentials. A similar statement can also be made for the wide spread perception on the role of discrete symmetries of the microscopic Hamiltonians. While they definitely are important as we demonstrate in the present work, there is no direct connection between the Cartan classification of the microscopic random Hamiltonian and the localisation properties. At this stage, the true reason why the transport follows different types for different random potentials remains inconclusive.

Disclosure statement

No potential conflict of interest was reported by the authors.

Funding

This work was supported by a grant of the Julian Schwinger Foundation for Physical Research.

References

[1] E. Abrahams, P.W. Anderson, D.C. Licciardello, and T.V. Ramakrishnan, *Scaling theory of localization: Absence of quantum diffusion in two dimensions*, Phys. Rev. Lett. 42 (1979), pp. 673–676.

[2] L.G. Gor'kov, A.I. Larkin, and D.E. Khmel'nitskii, *Particle conductivity in a two-dimensional random potential*, Pis'ma Zh. Eksp. Teor. Fiz. 30 (1979), pp. 248–252 [JETP Lett. 30 (1979), pp. 228–232].

[3] S. Hikami, A. Larkin, and Y. Nagaoka, *Spin-orbit interaction and magnetoresistance in the two dimensional random system*, Prog. Theor. Phys. 63 (1980), pp. 707–710.

[4] D. Vollhardt and P. Wölfle, *Diagrammatic, self-consistent treatment of the Anderson localization problem in $d \leqslant 2$ dimensions*, Phys. Rev. B 22 (1980), pp. 4666–4679.

[5] Y. Hanein, U. Meirav, D. Shahar, C.C. Li, D.C. Tsui, and H. Shtrikman, *The metalliclike conductivity of a two-dimensional hole system*, Phys. Rev. Lett. 80 (1998), pp. 1288–1291.

[6] K.S. Novoselov, A.K. Geim, S.V. Morozov, D. Jiang, M.I. Katsnelson, I.V. Grigorieva, S.V. Dubonos, and A.A. Firsov, *Two-dimensional gas of massless Dirac fermions in graphene*, Nature 438 (2005), pp. 197–200.

[7] Y.-W. Tan, Y. Zhang, K. Bolotin, Y. Zhao, S. Adam, E.H. Hwang, and S. Das, *Sarma, H.L. Stormer, and P. Kim, It Measurement of scattering rate and minimum conductivity in graphene*, Phys. Rev. Lett. 99(246803) (2007), pp. 1–4.

[8] D.C. Elias, R.R. Nair, T.M.G. Mohiuddin, S.V. Morozov, P. Blake, M.P. Halsall, A.C. Ferrari, D.W. Boukhvalov, M.I. Katsnelson, A.K. Geim, and K.S. Novoselov, *Control of graphene's properties by reversible hydrogenation: Evidence for graphane*, Science 323 (2009), pp. 610–613.

[9] M.J. Allen, V.C. Tung, and R.B. Kaner, *Honeycomb carbon: A review of graphene*, Chem. Rev. 110 (2010), pp. 132–145.

[10] L. Chen, Ch-Ch Liu, B. Feng, X. He, P. Cheng, Z. Ding, Sh. Meng, Y. Yao, and K. Wu, *Evidence for Dirac fermions in a honeycomb lattice based on silicon*, Phys. Rev. Lett. 109(056804) (2012), pp. 1–5.

[11] M.Z. Hasan and C.L. Mele, *Colloquium: Topological insulators*, Rev. Mod. Phys. 82 (2010), pp. 3045–3067.

[12] X.-L. Qi and S.-C. Zhang, *Topological insulators and superconductors*, Rev. Mod. Phys. 83 (2011), pp. 1057–1110.

[13] N.H. Shon and T. Ando, *Quantum transport in two-dimensional graphite system*, J. Phys. Soc. Jap. 67 (1998), pp. 2421–2429.

[14] T. Ando, Y. Zheng, and H. Suzuura, *Dynamical conductivity and zero-mode anomaly in honeycomb lattices*, J. Phys. Soc. Japan 71 (2002), pp. 1318–1324.

[15] H. Suzuura and T. Ando, *Crossover from symplectic to orthogonal class in a two-dimensional honeycomb lattice*, Phys. Rev. Lett. 89(266603) (2002), pp. 1–4.

[16] E. McCann, K. Kechedzhi, V.I. Fal'ko, H. Suzuura, T. Ando, and B.L. Altshuler, *Weak-localization magnetoresistance and valley symmetry in graphene*, Phys. Rev. Lett. 97(146805) (2006), pp. 1–4.

[17] D.V. Khveshchenko, *Electron localization properties in graphene*, Phys. Rev. Lett. 97(036802) (2006), pp. 1–4.

[18] B.L. Altshuler, A.G. Aronov, A.I. Larkin, and D.E. Khmel'nitskii, *Anomalous magnetoresistance in semiconductors*, Th. Eksp. Teor. Fiz. 81 (1981), pp. 768–776 [Sov. Phys. JETP 54 (1981), pp. 411–419].

[19] G. Tkachov and E.M. Hankiewicz, *Weak antilocalization in HgTe quantum wells and topological surface states: Massive versus massless Dirac fermions*, Phys. Rev. B 84(035444) (2011), pp. 1–13.

[20] D. Schmeltzer and A. Saxena, *Interference effects for $T^2 = -1$ time reversal invariant topological insulators: Surface optical and Raman conductivity*, Phys. Rev. B 88(035140) (2013), pp. 1–16.

[21] B.L. Altshuler and B.D. Simons, *Universalities: From Anderson localization to quantum chaos*, in *Mesoscopic quantum physics, Les Houches 1994*, E. Akkermans, G. Montambaux, J.-L. Pichard, and J. Zinn-Justin, eds., North Holland, Amsterdam, 1995, pp. 1–98.

[22] K. Efetov, *Supersymmetry in Disorder and Chaos*, Cambridge University Press, Cambridge, 1997.

[23] L.S. Levitov and A.V. Shytov, Green's functions. Theory and practice, Fizmatlit-Nauka, Moscow (2002). in Russian. Available at http://www.mit.edu/~levitov/book/.

[24] P.A. Lee, *Localized states in a d-wave superconductor*, Phys. Rev. Lett. 71 (1993), pp. 1887–1890.

[25] F.J. Wegner, *Disordered system with n orbitals per site: $n = \infty$ limit*, Phys. Rev. B 19 (1979), pp. 783–792.
[26] A.J. McKane and M. Stone, *Localization as an alternative to Goldstone's theorem*, Ann. Phys. 131 (1981), pp. 36–55.
[27] E. Fradkin, *Critical behavior of disordered degenerate semiconductors. I. Models, symmetries, and formalism*, Phys. Rev. B 33 (1986), pp. 3257–3262.
[28] E. Fradkin, *Critical behavior of disordered degenerate semiconductors. II. Spectrum and transport properties in mean-field theory*, Phys. Rev. B 33 (1986), pp. 3263–3268.
[29] K. Ziegler, *Scaling behavior and universality near the quantum Hall transition*, Phys. Rev. B 55 (1997), pp. 10661–10670.
[30] K. Ziegler and G. Jug, *Is the peak value of σ_{xx} at the quantum Hall transition universal?*, Z. Phys. B 104 (1997), pp. 5–6.
[31] K. Ziegler, *Delocalization of 2D Dirac fermions: The role of a broken supersymmetry*, Phys. Rev. Lett. 80 (1998), pp. 3113–3116.
[32] F. Wegner, *The mobility edge problem: Continuous symmetry and a conjecture*, Z. Phys. B 35 (1979), pp. 207–210.
[33] L. Schäfer and F. Wegner, *Disordered system with n orbitals per site: Lagrange formulation, hyperbolic symmetry, and Goldstone modes*, Z. Phys. B 38 (1980), pp. 113–126.
[34] S. Hikami, *Anderson localization in a nonlinear-σ-model representation*, Phys. Rev. B 24 (1981), pp. 2671–2679.
[35] K. Ziegler, *Random-gap model for graphene and graphene bilayers*, Phys. Rev. Lett. 102(126802) (2009), pp. 1–4.
[36] K. Ziegler, *Diffusion in the random gap model of monolayer and bilayer graphene*, Phys. Rev. B 79(195424) (2009), pp. 1–11.
[37] K. Ziegler, *Quantum diffusion in two-dimensional random systems with particle-hole symmetry*, J. Phys. A: Math. Theor. 45(335001) (2012), pp. 1–12.
[38] K. Ziegler and A. Sinner, *Weak-localization approach to a 2D electron gas with a spectral node*, Phys. E 71 (2015), pp. 14–20.
[39] A. Sinner and K. Ziegler, *Finite-size scaling in a 2D disordered electron gas with spectral nodes*, J. Phys.: Cond. Mat. 28 (305701) (2016), pp. 1–7.
[40] A. Sinner and K. Ziegler, *Perturbative analysis of the conductivity in disordered monolayer and bilayer graphene*, Phys. Rev. B 84(233401) (2011), pp. 1–4.
[41] A. Sinner and K. Ziegler, *Linear response peculiarity of a two-dimensional Dirac electron gas at weak scattering*, Phys. Rev. B 89(024201) (2014), pp. 1–13.
[42] A. Sinner, A. Sedrakyan, and K. Ziegler, *Optical conductivity of graphene in the presence of random lattice deformations*, Phys. Rev. B 83(155115) (2011), pp. 1–8.
[43] K. Ziegler and A. Sinner, *Transport in finite graphene samples with a random gap*, Phys. Rev. B 81(241404R) (2010), pp. 1–3.
[44] A. Sinner and K. Ziegler, *Two-parameter scaling theory of transport near a spectral node*, Phys. Rev. B 90(174207) (2014), pp. 1–5.
[45] A. Sinner and K. Ziegler, *Renormalized transport properties of randomly gapped two-dimensional Dirac fermions*, Phys. Rev. B 86(155450) (2012), pp. 1–10.
[46] A.W.W. Ludwig, M.P.A. Fisher, R. Shankar, and G. Grinstein, *Integer quantum Hall transition: An alternative approach and exact results*, Phys. Rev. B 50 (1994), pp. 7526–7552.
[47] P.K. Wallace, *The band theory of graphite*, Phys. Rev. 71 (1947), pp. 622–634.
[48] G.W. Semenoff, *Condensed-matter simulation of a three-dimensional anomaly*, Phys. Rev. Lett. 53 (1984), pp. 2449–2452.

[49] A.A. Burkov, *Chiral anomaly and transport in Weyl metals*, J. Phys.: Condens. Matter 27(113201) (2015), pp. 1–18.
[50] K. Huang, *Statistical Mechanics*, Wiley Inc., New York, 1963.
[51] M.R. Zirnbauer, *Riemannian symmetric superspaces and their origin in random-matrix theory*, J. Math. Phys. 37 (1996), pp. 4986–5018.
[52] A. Altland and M. Zirnbauer, *Nonstandard symmetry classes in mesoscopic normal-superconducting hybrid structures*, Phys. Rev. B 55 (1997), pp. 1142–1161.
[53] D. Bernard and A. LeClair, *A classification of 2D random Dirac fermions*, J. Phys. A: Math. Gen. 35 (2002), pp. 2555–2567.
[54] D. Bernard, E.-A. Kim, and A. LeClair, *Edge states for topological insulators in two dimensions and their Luttinger-like liquids*, Phys. Rev. B 86(205116) (2012), pp. 1–9.
[55] B. Huckestein and A. Altland, *Quasi-particle density of states and Thouless conductance of disordered d-wave superconductors*, Physica B 329(1461) (2003), pp. 71–72.
[56] V.M. Pereira, F. Guinea, J.M.B. Lopes dos Santos, N.M.R. Peres, and A.H. Castro, *Neto, Disorder induced localized states in graphene*, Phys. Rev. Lett. 96(036801) (2006), pp. 1–4.
[57] Sh Wu, L. Jing, Q. Li, Q.W. Shi, J. Chen, H. Su, X. Wang, and J. Yang, *Average density of states in disordered graphene systems*, Phys. Rev. B 77(195411) (2008), pp. 1–7.
[58] I. Aleiner and K. Efetov, *Effect of disorder on transport in graphene*, Phys. Rev. Lett. 97(236801) (2006), pp. 1–4.
[59] R. Oppermann and F. Wegner, *Disordered system with n orbitals per site: $1/n$ expansion*, Z. Phys. B 34 (1979), pp. 327–348.
[60] K. Ziegler, *Scaling relation for the density of states of a disordered n-orbital model*, Phys. Lett. A 99 (1983), pp. 19–21.

Appendix 1. Diffusion and conductivity

Starting from the transition probability

$$P_{rr'}(t) = \sum_{j,j'} \langle |\langle r,j|e^{-iHt}|r',j'\rangle|^2 \rangle_g, \tag{A1}$$

with $\langle \cdots \rangle_g$ denoting the disorder averaging we can calculate the diffusion coefficient as

$$D = \lim_{\epsilon \to 0} \epsilon^2 \sum_r (r_k - r'_k)^2 \int_0^\infty \mathrm{d}t\, P_{rr'}(t) e^{-\epsilon t}\,. \tag{A2}$$

With the Green's function $G(z) = (H - z)^{-1}$, we can write for the integral

$$\int_0^\infty \mathrm{d}t\, P_{rr'}(t) e^{-\epsilon t} = \int \mathrm{d}E\, \mathrm{Tr}_d \left\{ G_{rr'}(E + i\epsilon) \left[G_{r'r}(E - i\epsilon) - G_{r'r}(E + i\epsilon) \right] \right\}, \tag{A3}$$

where Tr_d is the trace with respect to the spinor index. Only the contribution with poles on both sides of the real axis is relevant. Then we can write

$$D = \lim_{\epsilon \to 0} \epsilon^2 \sum_r (r_k - r'_k)^2 \int \mathrm{d}E\, \mathrm{Tr}_d \left[G_{rr'}(E + i\epsilon) G_{r'r}(E - i\epsilon) \right]. \tag{A4}$$

Appendix 2. Proof of Equation (13)

Our aim is to give a proof for Equation (13)

$$\det[i\epsilon 1 + H_0 + V] = \det[i\epsilon 1 + H_0^T - \mathcal{O}V\mathcal{O}], \tag{B1}$$

for $H_0^T = -\mathcal{O}H_0\mathcal{O}$, $\mathcal{O}\mathcal{O} = 1$ and $\mathrm{Tr}_d[H_0 + V] = 0$, that is

$$H_0^T - \mathcal{O}V\mathcal{O} = -\mathcal{O}[H_0 + V]\mathcal{O} \tag{B2}$$

Be λ_i and μ_i eigenvalues of matrices $i\epsilon 1 + H_0 + V$ and $i\epsilon 1 + H_0^T - \mathcal{O}V\mathcal{O}$, respectively, then Equation (B1) is equivalent to

$$\prod_{i=1}^{2N} \lambda_i = \prod_{i=1}^{2N} \mu_i. \tag{B3}$$

The eigenvalues in turn follow from the solutions of the corresponding secular equations

$$\det[(\lambda - i\epsilon)1 - H_0 - V] = 0 = \det[(\mu - i\epsilon)1 - H_0^T + \mathcal{O}V\mathcal{O}], \tag{B4}$$

such that $\lambda' = \lambda - i\epsilon$ and $\mu' = \mu - i\epsilon$ represent the eigenvalues of random Hamiltonians $H_0 + V$ and $H_0^T - \mathcal{O}V\mathcal{O}$, respectively, and therefore real numbers. Then with Equation (B2) follows

$$\det[\lambda' 1 - H_0 - V] = 0 = \det[\mu' 1 - H_0^T + \mathcal{O}V\mathcal{O}] = \det[\mathcal{O}(\mu' 1 + H_0 + V)\mathcal{O}], \tag{B5}$$

i.e.

$$\det[\lambda' 1 - H_0 - V] = 0 = \det[\mu' 1 + H_0 + V], \tag{B6}$$

which obviously implies $\lambda_i' = -\mu_i'$. Because random Hamiltonians are traceless, the eigenvalues of d-dimensional matrices always appear in bundles, each of which sums up to zero separately, e.g. in $d = 2$ there are only two with opposite sing; in our case $d = 4$ there are two pair with opposite sing $\lambda_i' \to \pm|\lambda_i'|$, i.e. $\mu_i' \to \mp|\lambda_i'|$. Then Equation (B3) becomes

$$\prod_{i=1}^{N} (i\epsilon + |\lambda_i|)(i\epsilon - |\lambda_i|) = \prod_{i=1}^{N} (i\epsilon - |\lambda_i|)(i\epsilon + |\lambda_i|),$$

which obviously proofs Equation (13).

Appendix 3. Embedding of the totally degenerated random potential

In order to imbed the totally degenerated disorder which couples to the matrix Σ_{00} into the functional integral formalism of Section 3 we use the fact that $\langle V^{2n+1}\rangle_g = 0$ for any integer n, i.e. the sign of the random potential in the Hamiltonian does not affect the ultimate results. Then we can write the two-particles Green's function as

$$\begin{aligned} K_{rr'} &= \frac{1}{2}\mathrm{Tr}_4 \left\langle [i\epsilon + H_0 + V]^{-1}_{rr'} [-i\epsilon + H_0 + V]^{-1}_{r'r} \right\rangle_g \\ &\quad + \frac{1}{2}\mathrm{Tr}_4 \left\langle [i\epsilon + H_0 - V]^{-1}_{rr'} [-i\epsilon + H_0 - V]^{-1}_{r'r} \right\rangle_g \\ &= \frac{1}{2}\mathrm{Tr}_8 \left\langle \begin{bmatrix} i\epsilon + H_0 + V & 0 \\ 0 & i\epsilon + H_0 - V \end{bmatrix}^{-1}_{rr'} \right. \\ &\qquad \left. \begin{bmatrix} -i\epsilon + H_0 + V & 0 \\ 0 & -i\epsilon + H_0 - V \end{bmatrix}^{-1}_{r'r} \right\rangle_g , \end{aligned} \tag{C1}$$

and carry out calculations in this extended representation.

Appendix 4. Dyson and Bethe–Salpeter equations in weak scattering regime

We briefly recapitulate the derivation of the disorder averaged Green's function for the case of weak scattering. To keep the notation simpler, here we use the symbol $\langle\cdots\rangle$ to denote the ensemble average. We start with the expansion of the microscopic Green's function into the geometric series:

$$G = [G_0^{-1} + V]^{-1} \sim G_0 - G_0 V G_0 + G_0 V G_0 V G_0 - G_0 V G_0 V G_0 V G_0 \cdots \tag{D1}$$

Applying the averaging procedure in accord with Equation (7) we may drop all terms containing odd powers of V. Then rearranging we get:

$$\begin{aligned}\langle G\rangle &= \langle G_0 + G_0 V G_0 V G_0 + G_0 V G_0 V G_0 V G_0 V G_0 \cdots\rangle \\ &= \langle G_0 + G_0 V G_0 V (G_0 + G_0 V G_0 V G_0 + G_0 V G_0 V G_0 V G_0 V G_0 \cdots)\rangle \\ &\sim G_0 + G_0\langle V G_0 V\rangle\langle G\rangle = G_0(1 + \langle V G_0 V\rangle\langle G\rangle),\end{aligned} \tag{D2}$$

where we made use of the weak scattering conjecture. This yields the renormalisation of G:

$$\langle G\rangle \sim \left(G_0^{-1} - \langle V G_0 V\rangle\right)^{-1} \sim \bar{G}. \tag{D3}$$

In an analogous fashion, we consider the two–particle Green's function:

$$\langle G^+ G^-\rangle = \left\langle \left([G_0^+]^{-1} + V\right)^{-1} \left([G_0^-]^{-1} + V\right)^{-1}\right\rangle. \tag{D4}$$

We expand the Green's function into the geometric series:

$$\begin{aligned}\langle G^+ G^-\rangle &= \left\langle \left(G_0^+ - G_0^+ V G_0^+ + G_0^+ V G_0^+ V G_0^+ \cdots\right)\left(G_0^- - G_0^- V G_0^- + G_0^- V G_0^- V G_0^- \cdots\right)\right\rangle \\ &= G_0^+ G_0^- + \langle (G_0^+ V G^+)(G_0^- V G^-)\rangle - G_0^+ G_0^- \langle V G^-\rangle - \langle G^+ V\rangle G_0^+ G_0^-.\end{aligned} \tag{D5}$$

For assumed weak scattering the last two terms are of the order zero and we may retain only first two terms which allow for self-consistency

$$\langle G^+ G^-\rangle \sim G_0^+ G_0^- + \langle (G_0^+ V G^+)(G_0^- V G^-)\rangle. \tag{D6}$$

Expanding it in a matrix basis and exploiting the weak scattering conjecture we furthermore have

$$\begin{aligned}\langle G^+_{ij} G^-_{kl}\rangle &\sim G^+_{0,ij} G^-_{0,kl} + \left\langle G^+_{0,ia} V_{ab} G^+_{bj} G^-_{0,k\alpha} V_{\alpha\beta} G^-_{\beta l}\right\rangle \\ &\sim G^+_{0,ij} G^-_{0,kl} + \left\langle G^+_{0,ia} V_{ab} G^-_{0,k\alpha} V_{\alpha\beta}\right\rangle \left\langle G^+_{bj} G^-_{\beta l}\right\rangle,\end{aligned} \tag{D7}$$

which then reversibly rewritten reads

$$\begin{aligned}G^+_{0,ij} G^-_{0,kl} &\sim \left[\delta_{ib}\delta_{k\beta} - \langle G^+_{0,ia} V_{ab} G^-_{0,k\alpha} V_{\alpha\beta}\rangle\right]\langle G^+_{bj} G^-_{\beta l}\rangle \\ &= \langle [1 - (G_0^+ V)(G_0^- V)]\rangle_{ik;b\beta}\langle G^+_{bj} G^-_{\beta l}\rangle.\end{aligned} \tag{D8}$$

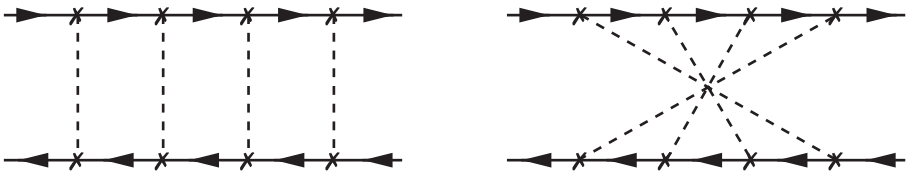

Figure D1. A generic diagram from the ladder (left) and from the maximally crossed (right) class.

The expression on the left-hand side is invariant under the averaging procedure, i.e. we can rewrite the last equation as follows:

$$\left\langle \left[1-(G_0^+V)(G_0^-V)\right]_{ik;b\beta}\left([1-(G_0^+V)(G_0^-V)]^{-1}_{b\beta;nm}G^+_{0,nj}G^-_{0,ml}-\langle G^+_{bj}G^-_{\beta l}\rangle\right)\right\rangle = 0. \quad \text{(D9)}$$

Making again use of the weak scattering conjecture we obtain the Bethe–Salpeter equation

$$\langle G^+_{nj}G^-_{ml}\rangle \sim \langle [1-(G_0^+V)(G_0^-V)]^{-1}\rangle_{nm;ik}G^+_{0,ij}G^-_{0,kl} \quad \text{(D10)}$$

which is the equation we have to evaluate. Expanding the disorder matrix in (D10) into the geometric series we get

$$\begin{aligned}&\langle [1-(G_0^+V)(G_0^-V)]^{-1}\rangle_{nm;ik}\\ &\quad=\delta_{ni}\delta_{mk}+\langle (G_0^+V)_{ni}(G_0^-V)_{mk}\rangle\\ &\qquad+\langle (G_0^+V)_{n\alpha}(G_0^-V)_{m\beta}(G_0^+V)_{\alpha i}(G_0^-V)_{\beta k}\rangle+\cdots. \end{aligned} \quad \text{(D11)}$$

Then performing the average in accord with Equation (7) by means of the Wick theorem we get

$$\begin{aligned}&\left\langle \left[1-(G_0^+V)(G_0^-V)\right]^{-1}\right\rangle_{nm;ik}\\ &\quad\sim\delta_{ni}\delta_{mk}+g\left(G_0^+\Sigma\right)_{ni}\left(G_0^-\Sigma\right)_{mk}\\ &\qquad+g^2\left[\left(G_0^+\Sigma\right)_{n\alpha}\left(G_0^+\Sigma\right)_{\alpha i}\right]\left[\left(G_0^-\Sigma\right)_{m\beta}\left(G_0^-\Sigma\right)_{\beta k}\right] &\text{(D12)}\\ &\qquad+g^2\left[\left(G_0^+\Sigma\right)_{n\alpha}\left(G_0^-\Sigma\right)_{m\beta}\right]\left[\left(G_0^+\Sigma\right)_{\alpha i}\left(G_0^-\Sigma\right)_{\beta k}\right] &\text{(D13)}\\ &\qquad+g^2\left[\left(G_0^+\Sigma\right)_{n\alpha}\left(G_0^-\Sigma\right)_{\beta k}\right]\left[\left(G_0^+\Sigma\right)_{\alpha i}\left(G_0^-\Sigma\right)_{m\beta}\right] &\text{(D14)}\\ &\qquad+\text{higher orders}.\end{aligned}$$

Line (D12) represents a self–energy contribution. The total effect arising from summing all diagrams in this class can be accounted by the replacement of naked propagators by the renormalised ones, i.e. $G_0^{\pm}\to\bar{G}^{\pm}$ via $\epsilon\to\epsilon+\eta$. The diagram class given by the complete geometric series

$$\begin{aligned}(1-t)^{-1}_{rr'|nm;ik}&=\delta_{rr'}\delta_{ni}\delta_{mk}+g\left[(G_0^+\Sigma)_{ni}(G_0^-\Sigma)_{mk}\right]_{rr'}\\ &\quad+g^2\left[[(G_0^+\Sigma)_{n\alpha}(G_0^-\Sigma)_{m\beta}][(G_0^+\Sigma)_{\alpha i}(G_0^-\Sigma)_{\beta k}]\right]_{rr'}+\cdots\\ &=\left[1-g(\bar{G}^+\Sigma)(\bar{G}^-\Sigma)\right]^{-1}_{rr'|nm;ik}, \end{aligned} \quad \text{(D15)}$$

is called the ladder class. The corresponding diagrammatic representation is shown in Figure D1 on the left. For manipulations in Line (D14) we note that $(\bar{G}^-\Sigma)_{ab}=(\bar{G}^-\Sigma)^T_{ba}$, where,

the transposition operator T applies to all degrees of freedom, i.e. to the spatial ones as well. This class of diagrams is called the maximally crossed class and is shown in Figure D1 on the right. This series is incomplete with missing zero and first order terms. Introducing them we can perform the summation of this diagram class, obtaining

$$\begin{aligned}(1-\tau)^{-1}_{rr'|nk;im} &= \delta_{rr'}\delta_{ni}\delta_{km} + g\left[(\bar{G}^{+}\Sigma)_{ni}(\bar{G}^{-}\Sigma)^{T}_{km}\right]_{rr'} \\ &\quad + g^2\left[[(\bar{G}^{+}\Sigma)_{n\alpha}(\bar{G}^{-}\Sigma)^{T}_{k\beta}][(\bar{G}^{+}\Sigma)_{\alpha i}(\bar{G}^{-}\Sigma)^{T}_{\beta m}]\right]_{rr'} + \cdots \\ &= \left[1 - g(\bar{G}^{+}\Sigma)(\bar{G}^{-}\Sigma)^{T}\right]^{-1}_{rr'|nk;im}. \end{aligned} \tag{D16}$$

Neglecting higher order diagrams we then obtain

$$\begin{aligned}\langle G^{+}_{nj}G^{-}_{ml}\rangle \sim \Big(&\left[1 - g(\bar{G}^{+}\Sigma)(\bar{G}^{-}\Sigma)\right]^{-1}_{nm;ik} + \left[1 - g(\bar{G}^{+}\Sigma)(\bar{G}^{-}\Sigma)^{T}\right]^{-1}_{nk;im} \\ &- \left[1 + g(\bar{G}^{+}\Sigma)(\bar{G}^{-}\Sigma)^{T}\right]_{nk;im}\Big)\bar{G}^{+}_{ij}\bar{G}^{-}_{kl}, \end{aligned} \tag{D17}$$

where first term in the parenthesis denote the ladder channel matrix, second term the maximally crossed channel matrix and the remaining terms are introduced in order to avoid the double counting. Addressing Equation (31) it is clear that none of the elements from the second line can develop a ϵ^{-2} singularity and thus disappear from the conductivity in the dc limit. Therefore, we ignore them in further analysis.

Appendix 5. A pecularity of the reduced Kubo formula Equation (54)

The reduced Kubo formula given in Equation (54) provides for a number of wrong predictions for nodal electrons. For instance, it yields a finite dc conductivity for the clean system with a gap in the spectrum. Indeed, at zero energy and in dc limit the Green's functions are simply

$$G_{\pm} = [-i\nabla\cdot\sigma + m\sigma_3]^{-1} \tag{E1}$$

and hence Equation (54) yields

$$\sigma_{\mu\mu} = \frac{e^2}{\hbar}\mathrm{Tr}\int\frac{d^2q}{(2\pi)^2}\,\frac{[q\cdot\sigma + m\sigma_3]\sigma_\mu[q\cdot\sigma + m\sigma_3]\sigma_\mu}{[q^2+m^2]^2} \sim \frac{e^2}{2\pi\hbar}. \tag{E2}$$

This strange result is solely because of the neglected contributions of the type $G_{\pm}\sigma_\mu G_{\pm}\sigma_\mu$, which annihilate it in the full Kubo formula:

$$\sigma_{\mu\mu} \sim \mathrm{Tr}\int\frac{d^2q}{(2\pi)^2}\,\left[G_{+}(q) - G_{-}(q)\right]v_\mu\left[G_{-}(q) - G_{+}(q)\right]v_\mu, \tag{E3}$$

if Equation (E1) is used. The equivalence of Equations (E3) and (9) for translationally invariant systems is easily shown using the matrix identities $G_{\pm}(q) - G_{\mp}(q) \sim 2i\epsilon G_{\pm}(q)G_{\mp}(q)$, the definition of the velocity operator $v \sim \nabla_q H$, and an integration by parts. Therefore, while studying transport in nodal systems, the full Kubo formula has to be used.